Evolution of the Corsica-Sardinia Batholith and late-orogenic shearing of the Variscides

Evolution of the Corsica–Sardinia Batholith and late-orogenic shearing of the Variscides

L. Casini[1,*], S. Cuccuru[1], A. Puccini[1], G. Oggiano[1], Ph. Rossi[2]

[1]DipNeT, University of Sassari, via Piandanna 4, 07100 - Sassari (Italy)

[2]BRGM, BP 6009, 45060 Orléans cedex 2, France

*Corresponding author (casini@uniss.it) phone +39 79228641

Abstract

The Corsica–Sardinia Batholith formed in the late Carboniferous–Permian along the northern Gondwana margin. One or more of the following processes may have raised the Variscan geotherm enhancing melting of the crust and uppermost mantle, such as: i) break-off and detachment of the Rheic oceanic slab, ii) mantle delamination due to gravitational re-equilibration of thickened crust, iii) shear heating, iv) advection of mantle-derived melts, and v) concentration of heat-producing elements. In this paper, we present a simple one-dimensional thermal model to explain the origin of the batholith in a geodynamic setting consistent with intraplate shearing between Gondwana and Cadomian-Avalonian blocks. Input parameters, and boundary and initial conditions of the model crust are derived from a careful re-examination of large petrological, geochronological, and structural datasets. All parameters are varied within a range of geologically realistic values to reproduce thermal histories related to different tectonic processes, and the reliability of models is quantitatively evaluated by comparing the simulated geotherms with a large dataset of pressure–temperature–time (P–T–t) constraints. The best fit to P–T–t constraints is obtained for: i) break-off in the Late Devonian-Early Carboniferous, ii) decreasing exhumation rates from 340 to 280 Ma, and iii) transpression at high average strain rates, mostly coeval with the peak of high-T–low-P metamorphism.

Keywords: crustal melting, Variscan shear zones, isotopes, U-Pb zircon age, numerical modeling

1. Introduction

Because of mechanical compatibility problems in the crust, conditions favoring the ascent of melts are mostly found within lithosphere-scale shear zones (Archanjo et al., 2008; Archanjo et al., 2013; Guimarães et al., 2011; Hollanda et al., 2010). Cordilleran-type batholiths (Ishihara, 1981) develop above subduction zones and are almost always characterized by relatively mafic melts with a strong mantle component. A reference example is the Jurassic to Cretaceous Californian Peninsular Range Batholith that formed above the Eastern Pacific subduction zone (Johnson et al., 2002; Lipman, 1992). Californian plutons are mostly rounded in map view and preserve only little evidence for emplacement-related deformation (Johnson et al., 2003; Johnson et al., 2002). Typical compositions of melts range from gabbro to quartz-diorite and tonalite, with the more felsic rocks being less abundant (Johnson et al., 2002; Lewis et al., 2001; Silver and Chappell, 1988). In contrast, continental batholiths formed during crustal reworking are composed of more felsic melts, often showing a dominant anatectic component. A large and well-known example of this type is the Borborema Province in northeastern Brazil, which formed in the Neoproterozoic in response to lithosphere-scale shearing within Gondwana (Archanjo et al., 2008; Archanjo et al., 2013; de Souza et al., 2006; Guimarães et al., 2011; Sá et al., 2002). Almost all plutons in the Borborema Province have a ribbon like shape with a mean aspect ratio of about 5, are internally homogeneous and range in composition from S-type leuco-granite to granodiorite, with the more mafic rocks such as gabbro and tonalite being less abundant .

This paper focuses on the evolution of the Corsica–Sardinia Batholith (C–SB), a large batholith developed along a network of late-Variscan (Carboniferous-Permian) crustal shear

zones bridging the northern Gondwana margin to central Europe (340–280 Ma; (Cocherie et al., 2005; Gaggero et al., 2007; Orsini, 1976; Paquette et al., 2003; Rossi and Cocherie, 1991)). The combination of excellent geological exposure, the absence of post-Variscan ductile deformation, and the existence of detailed geochemical, geochronological, and structural datasets make the C–SB an ideal candidate for testing models of pluton emplacement and crustal reworking. The remainder of this paper is organized as follows. First, we present a comprehensive review of existing datasets, including the geochronology of the main intrusive sequences (U2 and U3), the major, trace and rare-earth element (REE) compositions of melts, and the emplacement-related structures preserved in major plutons. Magmatic processes are discussed based on the structures observed at key locations in northern Sardinia where the source region, melt migration pathways, and emplacement sites are well exposed. The architecture of the C–SB is then compared with that of the two end-member batholith models; namely, the Cordilleran-type and continental batholiths. A general thermal model is inferred from petrological constraints and the timing of magmatic episodes. Finally, the applicability of different tectonic models to the evolution of the C–SB is tested using one-dimensional (1-D) thermal modeling, and the results are placed in the general context of geodynamic evolution of northern Gondwana during the Carboniferous–Permian transition.

2. Geological setting

The C–SB is a composite 500-km-long, 50-km-wide plutonic-volcanic province continuously exposed from northern Corsica to southeastern Sardinia (Fig. 1). In a restored pre-Permian paleogeography, the C–SB matches the position of the inferred boundary between Gondwana and southwestern Europe (Edel, 1980; Matte, 2001; von Raumer et al., 2012). However, because of its N–S orientation, the batholith is overall discordant with respect to both the

main tectonic lineaments such as the Posada–Asinara Line (PAL; Fig. 1) and, generally, the orogenic zonation acquired during the phase of crustal thickening (Carmignani et al., 1994; Conti et al., 2001). Based on field relationships, geochronological data, and petrological arguments, three magmatic suites can be distinguished in the C–SB (Ferré and Leake, 2001; Rossi and Cocherie, 1991): i) an early Mg–K calc-alkaline suite (U1) composed of monzo-diorites, monzonites, and subordinate ultrapotassic mafic rocks; ii) a composite, peraluminous to slightly peraluminous calc-alkaline suite (U2) composed of granodiorites and monzogranites with subordinate tholeiitic gabbros; and iii) a suite (U3) consisting of metaluminous calc-alkaline to calcic gabbros and alkaline volcanic complexes ranging in composition from basalt to rhyolite. The evolution of U1 rocks is usually explained in terms of the mixing of mantle-derived and lower crustal melts. Although these rocks might be able to record either slab break-off or delamination of the sub-continental lithosphere during the transition from thickening to extension (Ferré and Leake, 2001; Li et al., 2012), Mg–K plutons form only a small proportion of the C–SB and are excluded from further discussion.

The age of layered migmatites in northern Sardinia (350–345 Ma; (Ferrara et al., 1978; Giacomini et al., 2006) indicates that the beginning of anatexis under amphibolite facies conditions pre-dates the onset of emplacement of U2 plutons by at least 20 Myr, and is broadly coeval with the main phase of N–S shortening and nappe stacking in the external zones preserved in southern Sardinia (i.e., the Gerrei–Meana phase; (Conti et al., 2001)). Early U2 melts of tonalitic to granodioritic composition formed about 320 Ma (Casini et al., 2014; Casini et al., 2012). Based on U-Pb zircon ages of shear zones in northern Sardinia, the oldest U2 plutons (Oggiano et al., 2007) are mostly coeval with a phase of regional transpression also recorded in the French Massif Central (Faure et al., 2010). Between about 320 and 300 Ma, the composition of the granitic melts evolved to lower-MgO compositions, producing large granodioritic and monzogranitic massifs that form the bulk of the C–SB (Casini et al., 2012; Del Moro et al., 1975; Ferré and Leake, 2001; Oggiano et al., 2007;

Oggiano et al., 2005; Paquette et al., 2003). After the Carboniferous–Permian transition, U2 plutons were intruded by gabbroic sequences whose geochemical affinity is still debated (Bonin, 2004; Cocherie et al., 1994; Renna et al., 2006; Tommasini and Poli, 1992), and by coeval U3 A-type alkaline granites and volcanic complexes (Bonin et al., 1998; Egeberg et al., 1993; Poitrasson et al., 1995; Renna et al., 2013).

3. Evolution of the C–SB

The evolution of the C–SB is discussed below based on a comprehensive review of existing structural, geochronological, and geochemical datasets. Only recent U–Pb zircon ages and Ar/Ar data were used, to ensure the most accurate resolution of magmatic and tectonic events.

3.1.Structural setting: C–SB architecture

As a whole, the C–SB is discordant with respect to the general NW–SE structural trend acquired by the metamorphic basement during the phase of crustal thickening which spans the late Devonian and early Carboniferous (Carmignani et al., 1994; Conti et al., 2001). At the pluton scale, however, important differences arise between the U2 and U3 complexes. Most U2 plutons are ribbon-shaped (aspect ratio of 1:3 to 1:10 in map view) and with long axes oriented between N120° and N140°(Fig. 1), nearly parallel to the orogenic zonation and to the transpressional D2 structures (Carmignani et al., 1994; Carosi and Oggiano, 2002; Casini and Funedda, 2014; Casini et al., 2010). Although there is only poor evidence for post-magmatic deformation, U2 plutons have a generally well-developed flat magmatic foliation and a gently plunging lineation almost parallel to the metamorphic fabric of country rocks (Casini et al., 2012; Gattacceca et al., 2004). Most micro-granular mafic enclaves in U2 rocks are highly stretched along the magmatic fabric and have a tonalitic to granodioritic composition with biotite as the dominant Fe/Mg-bearing phase (Casini et al., 2012). Because

of the near-absence of Alpine deformation, the roots of the C–SB are easily recognized in northern Sardinia within remnants of the migmatitic–granulitic basement (Fig. 2) interleaved between early U2 plutons such as the Barrabisa and Isola di S. Maria granodiorites (Fig. 1). Close to the granodioritic plutons, layer-parallel leucosomes (Fig. 2a) tend first to collect in larger melt pockets controlled by the geometry of syn-magmatic shear zones (Fig. 2b); then, as the shear zones become increasingly linked, melt pockets evolve into larger sills (Fig. 2c). The plutons are inferred to originate from the coalescence of multiple sills, as is also proposed for other tonalitic–granodioritic intrusions in the C–SB (Kruhl and Vernon, 2005). In contrast, U3 complexes (Fig. 1) are elongated about N40°–60°, which is almost perpendicular to the orogenic structure (Casini et al., 2012; Gattacceca et al., 2004). These plutons show weak to nearly isotropic magmatic fabrics at the outcrop scale, and the contacts with older U2 plutons and metamorphic rocks are generally sharp (Fig. 2d). Micro-granular mafic enclaves are more abundant than in U2 plutons (1-5% vol.), mostly rounded, and are characterized by basaltic to dioritic compositions (Poli and Tommasini, 1999). Al-in-hornblende thermobarometry indicates that U3 plutons were emplaced at shallow crustal levels ($P < 0.2$ GPa), whereas U2 rocks record pressures in excess of 2.5 GPa (Casini et al., 2012). Shallower emplacement depth of U3 complexes is also confirmed by the presence of andalusite–cordierite-bearing mineral assemblages in metamorphic aureoles developed around mafic intrusions emplaced below Permian basins.

3.2.Geochronology: the timing of C–SB formation

The oldest plutons of the C–SB are the so-called HMK granites (high Mg-K) of northwestern Corsica (U1; Fig. 1). This suite of N–S-oriented plutons and sub-volcanic complexes was emplaced in a compressional setting (Laporte et al., 1991; Rossi et al., 1988) from 345to about 337 Ma (Paquette et al., 2003). After a period of quiescence, U2 magmatism started at

around 320 Ma as testified by the emplacement of small, peraluminous, cordierite–garnet-bearing granodiorites in northern Sardinia (Casini et al., 2012; Oggiano et al., 2007). The volumes of melts increased substantially at around 310–305 Ma, generating large monzogranitic massifs emplaced episodically within NW-SE oriented dilatant shear zones (U2; Fig. 1). U2 calc-alkaline magmatism lasted (Fig. 3) from 322 to about 285 Ma (Casini et al., 2012; Gaggero et al., 2007; Oggiano et al., 2007; Paquette et al., 2003). U–Pb zircon dating of single plutons suggests that the longevities of the associated magmatic systems were extremely variable, although there is a weak positive correlation between longevity and the volume of melt involved. Therefore, larger plutons such as the Arzachena massif in north Sardinia (Casini et al., 2012) or the Urbalaccone pluton of central Corsica (Paquette et al., 2003) represent long-lived systems (>5 Myr), whereas other plutons generally formed in a few million years (Paquette et al., 2003). The C–SB magmatic cycle ended between about 290 and 260 Ma (Fig. 3) with the emplacement of U3 alkaline granites and sub-volcanic complexes (Gaggero et al., 2007; Paquette et al., 2003). Although zircon ages suggest a partial overlap between U2 and U3 plutons, field relationships generally indicate that alkaline magmas were emplaced at shallow crustal levels, breaking through already cooled and partly exhumed U2 plutons.

3.3.Geochemistry: the compositions of U2 and U3 magmas

The geochemical compositions of the U2 and U3 complexes are discussed using recently published datasets (Barbey et al., 2008; Casini et al., 2012; Cocherie et al., 1994; Di Vincenzo et al., 1996; Poitrasson et al., 1995; Poitrasson et al., 1998; Poli et al., 1989; Poli and Tommasini, 1991; Renna et al., 2006, 2007; Secchi et al., 1991; Tommasini and Poli, 1992; Tribuzio et al., 2009). U2 granites are generally felsic rocks characterized by SiO_2 contents ranging from 53.56 to 77.14 wt.% (Fig. 4). U3 complexes show greater variability (SiO_2 between 42.5 and 77.73 wt.%) due to the presence of gabbroic–granodioritic mafic complexes

such as the Ota–Porto and Capo Falcone intrusions (Poli and Tommasini, 1991; Renna et al., 2006). The A/CNK ratio is almost uniform in U2 granites, with values ranging between 1.0 and 1.1, although in several places the ratio is above 1.1, indicating slightly peraluminous compositions.U3 complexes are characterized by extremely variable A/CNK ratios between 0.44 and1.17, with higher ratios generally being associated with higher SiO_2 contents (Poli and Tommasini, 1991; Renna et al., 2006).

This geochemical difference is even more apparent from Harker variation diagrams. U2 rocks define quite narrow trends, characterized by positive correlations for K_2O and Na_2O with SiO_2, marked negative correlations for MgO, CaO, P_2O_5, TiO_2, and Sr with SiO_2 (Fig. 4). Although U3 rocks with high SiO_2 content mostly overlap the trend of U2, samples are generally much more dispersed, and P_2O_5, TiO_2, Ba and Sr show bell-shaped, concave-down trends (Fig. 4).

The chondrite-normalized rare-earth element (REE) patterns for U2 and U3 are summarized in Fig. 5. U2 granites generally show a well-defined positive correlation between $\sum$REE and SiO_2; with lower values (46.15 ppm) in leucogranites and maximum values of around 304.52 ppm in granodiorites. The general REE pattern in U2 granites is characterized by slightly negative Eu anomalies, flat trends for heavy REE (HREE), and moderately enriched light REE (LREE), consistent with strong fractionation (La_N/Yb_N = 11.65). Both the Eu negative anomalies and LREE/HREE fractionation values generally increase with increasing SiO_2 content. The REE composition of U3 rocks is also positively correlated with SiO_2, and the total REE content is 14.31 ppm in gabbroic rocks and 302.22 ppm in monzogranite. The REE pattern for U3 rocks is similar to that observed for U2 granites, consisting of flat HREE trends and moderately enriched LREE. However, all samples of U3 rocks have much more pronounced negative Eu anomalies and the fractionation is about half that of the U2 rocks (La_N/Yb_N ranges from 0.37 to 25.2 with an average value of 5.28). The isotopic signatures of

granitic magmas in the C–SB display the following characteristics: i) $0.706 < Sr_i < 0.707$, ii) $-4.3 < \varepsilon Nd < -1$, and iii) $+7 < \delta^{18}O‰ < +8$ (Fig. 6). Various types of source have been proposed to account for the origin of U2 monzogranitic melts: i) non-modal batch partial melting of a protolith calculated as greywacke in composition (Cocherie, 1984; Cocherie et al., 1994); ii) a 25%–35% degree of melting of biotite–amphibolite (Poli et al., 1989); and iii) partial melting of a composite source made up of Ordovician calc-alkaline granitoids and sedimentary rocks, eventually contaminated by a small component of enriched mantle-derived melts (Tommasini and Poli, 1992).

4. Thermal modeling

Based on petrological constraints, the C–SB is generally inferred to have a strong anatectic component (Ferré and Leake, 2001; Rossi and Cocherie, 1991).The high temperature–low pressure (HT–LP) gradient required to induce extensive melting of the crust may be generated by selective enrichment of heat-producing elements, slab break-off, advection of hot mantle-derived melts, or shear heating (Burg and Gerya, 2005). All these mechanisms are evaluated in the present study using a suite of Matlab-derived codes based on the finite differences method (Casini, 2012; Casini et al., 2013). Although this paper focuses on the late Carboniferous–early Permian U2 and U3 magmatic events, simulations are performed within a longer time span (between 350 and 280 Ma) to avoid numerical artifacts related to the initial conditions. This allows the initial modeled crust to be set up using relatively well-constrained parameters typical of the thickening phase, instead of more restrictive initial conditions.

4.1.Modeling strategy

The heat conduction equation is formulated in one dimension, assuming temperature-dependent thermal conductivity (Vosteen and Schellschmidt, 2003; Whittington et al., 2009) and heat sources, as follows:

$$\partial T/\partial t = 1/C_p\rho\partial z^2\partial/\partial z(\kappa\partial T/\partial z) + H/C_p\rho \quad (1)$$

where T is temperature (K), t is time (s), κ is thermal conductivity (m^2s^{-1}), C_p is specific heat ($Jkg^{-1}°C^{-1}$), ρ is density (kgm^{-3}), z is depth (m), and the term $H = (H_r+H_s)$ represents the volumetric heat production rate (Wm^{-3}) due to the decay of radioactive elements (H_r) and shear heating (H_s). $\sigma\dot{\varepsilon}$ Dirichlet boundary conditions are imposed at both ends of the model profile, and therefore we assume a constant temperature of 0°C at the surface and 2050°C at 1650 km depth. This gives a linear temperature gradient of about 0.5°C/km in the mantle and a temperature of 1350°C at the base of a 200-km-thick stable lithosphere. Slab break-off is reproduced by raising the temperature of a 12-km-thick section of the upper mantle located about 20 km beneath the Moho, to 1350°C; this implies a nearly instantaneous upwelling of hot asthenosphere. The initial temperature profile is calculated from the steady-state solution of Equation 1 given a starting configuration of the model crust which reflects thermal equilibrium at the end of thickening (Table 1). Transient solutions of Equation 1 are approximated on a numerical grid using a fully implicit finite-difference algorithm derived from (Casini, 2012). The grid consists of 151 irregularly spaced nodes, of which the first 101 are closely spaced in the lithosphere and the last 50 are distributed in the sub-lithospheric mantle, from the astenosphere to 1650 km depth. This setting provides an optimal resolution (of 0.7 to 0.4 km) in the crust and makes the code very efficient even for small time steps (< 0.1 Myr).

4.2.Partial melting

Partial melting is allowed in the section of the profile crossing the solidus–liquidus curves of crustal rocks, represented by wet granite for the upper crust (Johannes and Holtz, 1996) and dry tonalite for the lower crust (Patino Douce, 2004). This assumption is consistent with the trondhjemitic to tonalitic composition of early melts in migmatitic massifs (Cruciani et al., 2008) dated around 350 Ma (Ferrara et al., 1978; Giacomini et al., 2005). To a first approximation, the proportion of melt ϕ in crustal rocks is assumed to be independent of time and to increase linearly with T as follows (Burg and Gerya, 2005):

$$\begin{cases} \phi = 0 \; if \; T < T_s \\ \phi = \left(\frac{T_r - T_s}{T_l - T_s}\right) \; if \; T_s < T < T_l \\ \phi = 1 \; if \; T > T_l \end{cases} \qquad (2)$$

where T_s and T_l represent the solidus and liquidus temperatures, respectively. The melt proportion (ϕ) in the crust is dynamically evaluated at each time step based on the current temperature distribution. Heating due to upward melt migration is accounted for by assuming that melt cannot escape its source region until the melt-to-solid ratio reaches a critical value of $\phi = 0.06$ (Vogt et al., 2012). Once this value is exceeded, all melt above a non-extractable amount of $\phi_{min} = 0.02$ flows almost instantaneously upward through dykes (Petford et al., 2000), accumulating around the contemporary 350°C isotherm. Our model neglects the endothermic nature of melting reactions. Therefore, rapid advection of these lower crustal melts has two obvious consequences: i) an increase in the thickness of upper crust and a proportional decrease in the thickness of lower crust and ii) local perturbation of the conductive geotherm , characterized by heating at shallow levels while the lower crust might remains close to the solidus temperature. The amount of melt at every node at time $t = t^n$ is computed, taking into account the cumulative volume of already-extracted melt, $\phi^n = \sum_{i=1}^{n-1} \phi^i$, and therefore layers become refractory and eventually melting stops when ϕ^n exceeds a standard ϕ_0 value of extractable melt (Vogt et al., 2012).The statistical accuracy of

the results is evaluated at each time step based on the available thermobarometric constraints for the Moldanubian domain of southern Europe (Appendix A – Supplementary material). The relative error is thus calculated as the median difference between a best-fit polynomial for the pressure–temperature–time (P–T–t) constraints and the calculated geotherms over a region of interest. Therefore, negative errors indicate that temperature is overestimated, and vice versa.

4.3.Shear heating

Thermal models account for strike-slip deformation within a vertical fault extending from the brittle-ductile transition zone to the Moho. This assumption is consistent with the kinematic of late-Variscan structures widely exposed within the south Variscides (Casini et al., 2012; Matte, 2001; Rossi et al., 2009). For simplicity, we neglect the thermal effect of brittle processes involving fracturing, pseudotachylite development and rock pulverization (Ben-Zion and Sammis, 2012). In other words, the component H_s accounts only for viscous deformation; therefore, the results might provide a conservative estimate. Shear heating is calculated as (Burg and Gerya, 2005; Turcotte and Schubert, 2002)

$$H_s = \sigma_y \dot{\varepsilon} \quad (3)$$

where σy is yield stress (MPa) and $\dot{\varepsilon}$ is the viscous strain rate (s^{-1}) supported by a vertical shear zone below the 300°C geotherm. Deformation is activated when the node temperature exceeds the threshold for thermally-activated creep processes and the yield stress is calculated from the flow laws for dislocation creep of quartzite (Gleason and Tullis, 1995) and plagioclase An_{50} (Ranalli, 1995) for upper crustal and lower crustal rocks, respectively. Strain rate is calculated at each nodes as (Platt and Behr, 2011):

$$\dot{\varepsilon} = \frac{V}{w} \quad (4)$$

where V is average displacement velocity (ms^{-1}) and w is the shear zone width (m). At steady-state the shear zone width is constant and deformation is assumed to switch from power-law dislocation creep to linear diffusional processes, yielding to a decrease of stress; therefore, w is calculated at each nodes from Eq. 4 by substituting strain rate with stress values related to pressure-solution or diffusion creep (σ_{diff}):

$$w = \frac{V}{\sigma_{diff}} \quad (5)$$

4.4.Experimental set-up

Compositional parameters of the crustal model, such as the density, median and standard deviation to heat production rate of layers (Table 1),were determined on the basis of published datasets (Cocherie et al., 1994; Lucazeau and Mailhe, 1986; Ray et al., 2006; Verdoya et al., 1998). The initial (350 Ma) model crust is divided into three layers (Table 2) constrained by combining geophysical information and petrological observations. Deep seismic profiles through the south Variscan crust show a present-day Moho depth of about 36–43 km, with the greatest depths being preserved in regions unaffected by post-Variscan extension (Grad and Tiira, 2009). The Variscan lithosphere is generally thought to have reached a stable configuration in the early Permian, so a Moho depth of 41 km is imposed as a boundary condition at the end of the experiments (280 Ma). A reference bulk crustal thickness of 70 km (L_{bulk}) is assumed at the beginning of the experiments (350 Ma), to match the petrological constraints given by high pressure granulites (O'Brien and Rotzler, 2003). Based on the inferred maximum thickness of Carboniferous syn-orogenic basins preserved in this region of the Variscan chain (Echtler and Malavieille, 1990), the thickness of the sedimentary part of the upper crust (layer1 or L_1) is set to 7 km in the early Carboniferous. Because most of the late Carboniferous and early Permian granitic melts were sourced in the lower crust (Ferré

and Leake, 2001; Rossi and Cocherie, 1991), the initial thickness of the lower crust beneath the incoming C–SB (layer 3 or L_3) is assumed to be 28 km to balance the volume of removed material (Caggianelli and Prosser, 2003; Finetti, 2005).The initial thickness of the metamorphic part of the upper crust (layer 2 or L_2) is calculated by difference as $L_2 = L_{bulk} - (L_3+L_1) = 35$ km. The additive effects of slab break-off and shear heating are evaluated in 18 numerical experiments that employ variable exhumation rates and shear intensities (Table 2).

In the first three experiments, performed under a constant exhumation rate, we assume variable heat production rate of the lower crustal layer (experiments r0a-c, Table 2). Slab break-off and shear are not simulated to evaluate the effect of selective enrichment of heat-producing elements in the crust. In the following five experiments, still performed at constant exhumation rate, slab break-off is imposed from 340 to 300 Ma at intervals of 10 Myr. The rate of crustal exhumation between 340 and 280 Ma is set to a constant value of 0.72 mm/y, whereas shear strain is assumed to be absent (experiments r1–r5, Table 3). The second set of experiments (r6–r10, Table 2) uses similarly constant exhumation rates, but nodes in the ductile region of the model are subjected to shear strain. . In all experiments, the peak strain rates recorded by the uppermost ductile node of the model crust range from $10^{-15}$to about $10^{-13}s^{-1}$, consistent with geochronological constraints and the observed cutoff (Carosi et al., 2012; Casini et al., 2012; Matte, 2001). In experiments r6–r10, slab break-off is simulated to occur at 345 Ma, some 5–10 Myr before the emplacement of U1 plutons in northwestern Corsica (Paquette et al., 2003). The set of experiments from r11 to r18 evaluates the effect of varying the exhumation rates of the Variscan crust. In these experiments, slab break-off occurs at 345 Ma, and ductile shearing of the lithosphere is imposed between 322 and 305 at an average rate of 10^{-13}or $10^{-12.9}s^{-1}$. Based on published P–T–t paths (Casini et al., 2010; Faure et al., 2010; Giacomini et al., 2006), exhumation rates are varied over about two orders of magnitude, from 1.30 to 0.01 mm/y. Four different exhumation rate histories are simulated

(Table 2): i) continuously increasing (r11), ii) continuously decreasing (r15–r18), iii) increasing in a step-like manner (r12), and iv) decreasing in a step-like manner (r13–r14).

4.5.Results

The first set of model runs (Fig. 7a-c) indicates that the Carboniferous petrological constraints (Fig. 7a-b) can be reasonably fitted for a lower crust characterized by a high, though realistic, heat production rate of 0.6 μWm^{-3} (experiment r0b, Table 2). This value gives a somewhat low Permian (280 Ma) surface heat flow, Q_s, of about 80 mWm^{-2} (Table 2); therefore, the 280 Ma geotherm is underestimated by about 40-60°C (Table 3), while the final thickness of the lower crust is 5 – 7 km above the inferred present-day value of 17.5 km (Finetti, 2005). Permian constraints might be correctly reproduced for lower crustal heat production rates above 0.8 μWm^{-3} (Fig. 7c). In this model (experiment r0c, Table 2), melting begins about 340 Ma and the crust remains close to its solidus temperature for about 12 Myrs, yielding to a final lower crustal thickness which is very close to the actual value. However, model r0c overestimates by 80 – 150°C the Carboniferous geotherm. The following experiments (Fig. 7d–f, experiments r1-r5) conducted at constant exhumation rates and a variable age of slab break-off show that the best fit to petrological constraints is obtained for break-off in the early Carboniferous (345 Ma). This is particularly evident before 325 Ma, as the calculated geotherms underestimate by about 100–150°C the temperature recorded in the granulitic lower crust (Fig. 7d). In all of these experiments, the final (280 Ma) thickness of the lower crust is between about 18 and 21 km, and the surface heat flow ranges between 98 and 105 mWm^{-2} (Table 2). . The timing of the beginning of anatexis changes from 318 to 302 Ma for

progressively younger ages of break-off but remains largely consistent with the ages of U2 plutons in the C–SB (Table 2).

The experiments r6-r10 (Fig. 7g–i) involve a change in the shallow geotherm for variable strain rates and timing of shear. The models that best fit thermobarometric constraints between 320 and 290 Ma require a relatively high strain rate ($10^{-14}$to $10^{-12.8}s^{-1}$) applied between about 320 and 310 Ma (Table 2). Experiments characterized by lower strain rates overestimate the temperature indicated by thermobarometric constraints at around 300 Ma (Fig. 7h), whereas temperatures in the early Permian are underestimated (Fig. 7i). Anatexis starts between 321 and 317 Ma. Partial melting is generally rapid (<10 Myr) and the final thickness of the granulitic lower crust is about 18.2 km for surface heat flow in the range of 99 – 108 mWm^{-2} (Table 2).

Experiments r11 to r18 simulate the effect of variable exhumation histories. The results obtained by combining different exhumation histories are shown in Fig. 7l–n. Regardless of the early Carboniferous evolution, calculated geotherms are all consistent (errors between about +1% and −7%) with the P–T conditions during the emplacement of U1 plutons (Fig. 8). After about 325 Ma, at the onset of U2 magmatism, the behavior of the geotherms is largely dependent on the assumed exhumation path. Continuous and step-like increases in exhumation rates produce indistinguishable results. In both the continuous and step-like cases, anatexis starts at around 325 Ma and the lower crust reaches a final thickness of about 18.5 km, close to the preferred value for the early Permian. However, temperature is persistently overestimated in the upper 30 km of the crust, and a final Moho temperature of about 1000°C is generated (Fig. 7l). A step-like decrease in exhumation rates causes limited melting at around 300 Ma, and produces a final thickness of the lower crust of about 25 km and a final Moho temperature of about 900°C (Fig. 7m). Although the relative errors are lowest at around 320 Ma, temperature is increasingly underestimated (errors between about +5% and +15%) at

shallow crustal levels after about 290 Ma, close to the emplacement ages of the U3 magmatic sequence (Fig. 8). Results based on progressively decreasing exhumation rates(r18; Fig. 7n) show that melting is extensive between about 318 and 311 Ma. Anatexis causes the lower crust to reach a stable thickness of 18.2 km at 10 Myr before the Permian, with a final Moho temperature of 850–900°C (Fig. 7n). Although the relative errors at around 320 Ma are somewhat larger than those calculated assuming a step-like decrease of exhumation rates, experiment r18 provides the best fit to P–T–t data (Fig. 8; Appendix A – supplementary material).

5. Discussion

5.1.Emplacement mechanisms and tectonic setting

Based on the revised geochronology of the C–SB, structural and AMS (Anisotropy of Magnetic Susceptibility) studies suggest that the dominant emplacement mechanism changed across the Carboniferous–Permian transition, pre-dating by a few million years the onset of U3 magmatism. Carboniferous U2 plutons were emplaced at shallow depths ($P < 0.4$ GPa; (Casini et al., 2012; Laporte et al., 1991)), forming elliptical bodies characterized by a horizontal foliation and a sub-horizontal magmatic lineation acquired during orogen-parallel extension. The spatial correspondence of U2 plutons with late Carboniferous shear zones dated at about 325–305 Ma in northern Sardinia (Carosi et al., 2012; Di Vincenzo, 2004) supports a model of emplacement through channelized flow within ductile shear zones (Casini et al., 2012), as proposed for late Variscan granites in the French Massif Central (Faure et al., 2010), for the Armorican Massif (Bellot, 2007), and for the analogous domain in the Iberian

Massif (Vilà et al., 2005). However, the development of horizontal magmatic foliations (Gattacceca et al., 2004) indicates that shear zones represent efficient pathways for melt migration rather than sites of emplacement.

Based on these observations, we argue that U2 plutons developed in the extending part of the upper crust as a consequence of rapid, probably episodic, melt migration focused by ductile shear zones rooted in the lower crust (Fig. 9). A model of crustal-scale shearing is fit to explain the observed offsets of the orogenic structure, as well as most features of late Carboniferous paleo-geographic models for the south Variscan chain (Matte, 2001; Pereira et al., 2010). In contrast, lower Permian U2 and U3 plutons show a completely different architecture consistent with orogen-perpendicular extension (Gattacceca et al., 2004). In most cases, these intrusions are characterized by: i) sharp contacts with either the metamorphic basement and the older granites, ii) weak development of an internal fabric, and iii) the presence of stoped blocks in the pluton roof zone. Therefore, we argue that the emplacement of post-Carboniferous plutons was dominated by buoyancy in the absence of regional deformation, yielding to diapirism and ballooning (Johnson et al., 2003; Paterson et al., 1989). This interpretation is further supported by the common occurrence of rounded, non-oriented, mafic enclaves (Barbey et al., 2008), which indicate a nearly isotropic state of stress within magma chambers. Based on these arguments, we propose that the late phase of construction of the C–SB occurred in a general context of post-orogenic crustal extension.

5.2.Thermal regime

The numerical simulations showing the best fit to the early Carboniferous thermobarometric constraints require the oceanic slab to break off relatively early, between 345 and 335 Ma.

The assumption of younger ages cause a substantial underestimation of temperature in the granulitic lower crust at around 330 Ma and an overestimation after the Carboniferous–Permian transition due to the development of unrealistically high temperatures (>1000°C) at the base of the crust. Petrological models for U1 magmatism are in good agreement with this interpretation. In fact, the peculiar geochemistry and isotopic compositions of Mg–K melts have been explained in terms of rapid melting of the crust–mantle interface beneath a 60–70-km-thick crust (Ferré and Leake, 2001; Lexa et al., 2011). Given the solidus temperature of peridotite at about 2 GPa, partial melting of the sub-continental mantle requires a positive thermal anomaly that can likely be explained in terms of upwelling of partially molten asthenosphere at a temperature of 1300-1400°C. Based on the ages of U1 plutons (Paquette et al., 2003), break-off is assumed to have taken place at around 345 Ma because of the 5–10 Myr relaxation time needed to recover a near-equilibrium geotherm (Huw Davies and von Blanckenburg, 1995).The best fit to P–T–t conditions recorded for around 320 Ma is controlled primarily by the duration and magnitude of shear heating, as both the volume of melts and the age of anatexis changes as a function of deformation. Geologically meaningful results are obtained for high strain rates of $10^{-12.9}s^{-1}$applied between 320 and 312 Ma; lower rates generate temperatures that are too low at around 305 Ma and do not generate sufficient melting of the lower crust (Fig. 7h, n). Although extrapolation of averaged strain rates is subject to several uncertainties related to the effective rheology of shear zones (Handy, 1994), the suggested values are consistent with the strain rates extrapolated from late Variscan shear zones close to the southern edge of the C–SB (Casini et al., 2010). The role of shear heating is further supported by the age and duration of anatexis in model r18, which are in excellent agreement with the U–Pb zircon ages of most early U2 plutons (Casini et al., 2012; Oggiano et al., 2007; Paquette et al., 2003). Experiments conducted at variable rates of exhumation suggest that the thermal regime established after the Carboniferous–Permian transition depends on the inferred exhumation path. Based on the results of model r13, the almost-

complete exhumation of the southern Variscan crust prior to320 Ma can be dismissed because of the extremely inefficient melting of the lower crust that would prevent the C–SB from forming. This observation is broadly consistent with the overall exhumation history of the south Variscan crust, as rapid uplift and the development of metamorphic core complexes occurred mostly between 310 and 300 Ma (Casini and Oggiano, 2008; Faure et al., 2010).The best fit to P–T–t data is thus obtained for slab break-off in the early Carboniferous, for intense shearing from 320 to about 310 Ma, and for exhumation rates progressively decreasing from about 1.00 to 0.05 mm/y (Fig. 7n).

5.3.Geodynamic interpretation

The proposed model for the evolution of the C–SB provides constraints on the controversial issue of the origin of the early Permian thermal anomaly and late Variscan geodynamics in southern Europe. Indeed, any model accounting for the magmatism and anatexis of the C–SB must fit the geological constraints imposed by adjacent domains.

Based on the anomalously high geothermal gradient and the age of peak mineral assemblages, most researchers consider that HT metamorphism and crustal melting in the south Variscan crust took place in an overall extensional tectonic setting (Carmignani et al., 1994; Echtler and Malavieille, 1990; Ferré and Leake, 2001). Four major processes might have contributed to steepen the geotherm during crustal extension: (i) selective enrichment of radiogenic heat-producing elements in the crust caused by gravitational collapse of a thickened crustal wedge (Grad and Tiira, 2009) upwelling of hot asthenosphere due to slab break-off, (iii) focused shear heating (i.e., localized, intense shear heating of short duration) related to the

development of lithosphere-scale shear zones, or (iv) advection of hot mantle-derived magmas.

Enhanced radiogenic heat production may cause HT metamorphism and anatexis in regions of thickened crust after an incubation time on the order of 40-100 Myrs (Alcock et al., 2009; Brouwer et al., 2004; Liu, 2001). However, it is considered that concentration of heat-producing elements in the crust alone cannot account for the thermal anomaly in the south Variscan crust because C–SB plutons and the metamorphic basement of the Corsica–Sardinia block are only slightly enriched in radioactive elements; moreover, the existent heat flow studies contradict the hypothesis of a crust anomalously enriched in radiogenic heat-producing elements (Lucazeau and Mailhe, 1986; Verdoya et al., 1998). This conclusion is also supported by the age of U2 magmatism, which followed the main phase of crustal shortening by less than 50 Myr.

The results of numerical modeling presented in this paper suggest that slab break-off represents a viable mechanism for generating HT conditions at the base of a thickened Variscan crust. However, P–T conditions recorded by HP granulites and U1 magmatism can be fitted only for slab break-off prior to 340Ma, because of the short time-scale for generating a thermal anomaly through detachment of the lower part of the collided lithosphere (Huw Davies and von Blanckenburg, 1995). Results of numerical models that simulate subduction of continental lithosphere to mantle depths suggest that the oceanic plate usually detaches near the transition from oceanic to continental lithosphere at the end of continent–continent collision (Huw Davies and von Blanckenburg, 1995). The upward migration of hot, partially molten asthenosphere may cause the lower crust to start melting at some 5–10 Myr after detachment of the slab. In this context, partial mixing and hybridization of mantle-derived and lower crustal melts is expected. The available petrogenetic models for U1 magmatism and the ongoing compressional setting recorded by most plutons are largely consistent with this

interpretation (Ferré and Leake, 2001). Based on these data and inferences, it is proposed that the root zone of the southern Variscan belt experienced slab break-off in the early Carboniferous, some 5–10 Myr before the emplacement of U1 plutons (Fig. 10). Extensive partial melting of the lower crust suggests that slab break-off might have lowered the effective viscosity of the lower crust, enhancing the transition from crustal shortening to extension. However, recent studies of the Corsica–Sardinia migmatitic basement recognize a major phase of transpression between about 320 and 305 Ma (Carosi et al., 2012; Di Vincenzo, 2004; Oggiano et al., 2007), broadly coeval with the development of lithospheric-scale shear zones and anatexis in the French Massif Central (Faure et al., 2010), in the Maures–Esterel massif, and in the external crystalline massifs in the Alps (Rubatto et al., 2010). Paleomagnetic studies conducted in the C–SB region and surrounding areas support a general strike-slip model because of the large rotations recorded by the southern European Variscan crust (Fig. 10) at the end of the Carboniferous (Edel, 1980; Edel et al., 2014). The common association of U2 granites and HT ductile shear zones (Casini et al., 2012; Oggiano et al., 2007) is clearly at odds with models of generalized extension (Carmignani et al., 1994; von Raumer et al., 2012) and provides circumstantial evidence for a causal relationship between U2 magmatism and strike-slip tectonics. Localization of melting in shear zones (Fig. 9) may be explained in terms of a positive feedback effect between ductile deformation and temperature (Burg and Gerya, 2005; Nabelek and Liu, 1999), or efficient channelizing of melts within relatively low-pressure zones (Faure et al., 2010; Mancktelow, 2002). It is difficult to distinguish between these two possibilities in migmatitic complexes; however, high-resolution zircon ages and cross-cutting relationships between different plutons clearly illustrate the episodic nature of U2 magmatism (Paquette et al., 2003). Given the short duration of magmatic pulses and the crustal origin of melts, these data may indicate that either: i) a large portion of the lower crust in south Europe remained above the solidus temperature for about 25–30 Myr while the emplacement of plutons was controlled by

occasional development of shear zones; or ii) solidus temperatures in a generally hot, though melt-poor crust were episodically exceeded because of the rapid propagation of localized thermal anomalies. Option (i) implies the existence of a large thermal anomaly beneath the Moho, which does not explain either the inferred age of slab break-off or the scarcity of mantle-derived melts within U2 massifs. The model of episodic anatexis instead requires the propagation of several short-lived, localized, thermal pulses that can be interpreted in terms of shear heating. This conclusion is also supported by the results of numerical experiments conducted using geologically realistic strain rates and durations of ductile deformation (Fig. 7). For average strain rates on the order of 10^{-13} s^{-1}, temperature could have increased by some 30–80°C at shallow crustal levels, but even larger temperature increments are expected assuming repeated phases of shearing. These conclusions suggest that late Variscan shear zones might have actively contributed to the heat budget of the Variscan crust, supporting anatexis during the Carboniferous–Permian transition (Fig. 10). The volumetrically limited, but systematic, occurrence of gabbroic to quartz-dioritic U3 complexes at around 292–285 Ma (Fig. 3) suggests that the emplacement of mantle-derived magmas had a significant effect on the Variscan geotherm from the early Permian (Casini, 2012; Casini et al., 2012). U3 plutons and volcanic complexes fill SW–NE-oriented extensional domains equivalent to early Permian post-orogenic basins. The regular spacing of mafic complexes throughout the C–SB suggests distributed partial melting of the sub-continental mantle between 292 and 285 Ma, consistent with orogen-perpendicular extension (Fig. 10).

6. Conclusions

The evolution of the C–SB may not have involved a simple switch from crustal shortening to post-orogenic collapse of the thickened Variscan crust, although this model has became very popular over the past 40 years (Carmignani et al., 1994; Echtler and Malavieille, 1990; Matte, 2001). Stretching already-hot crust can result in decompression melting; however,

metamorphic P–T–t paths in northern Sardinia and southern Corsica (Giacomini et al., 2006; Giacomini et al., 2008) show that temperatures increased during the late Carboniferous, requiring additional heat sources. This can be explained either by a large thermal anomaly rooted in the sub-continental mantle, or by focused shear heating in an already attenuated, and presumably hot, crust. The first hypothesis, although realistic in a context of early crustal extension after slab breakoff, does not fit to explain the peculiar features of U2 magmatism. The Pennsylvanian age of most U2 massifs is, in fact, 25 – 40 Myrs younger than the end of collision, thus 2 to 4 times larger than the typical timescale for thermal relaxation after breakoff (Huw Davies and von Blanckenburg, 1995). Additional support to this interpretation is provided by the major element composition and isotopic signature of U2 melts. Although advection of mantle-derived liquids into a still hot lower crust might have enhanced melting, the composition of U2 massifs indicate that this contribution was probably minor. Therefore, we propose that the heat sources of late-Carboniferous U2 magmatism were mainly located in the crust2. Based on the results of numerical simulations, high (though realistic) strain rates in the order of 10^{-13} s^{-1} would have caused anatexis in a still hot, extending crust. Because long-lived shear zones likely accumulate strain as discrete increments rather than in a continuous way, an even larger positive feedback effect is expected between shear heating, temperature, and partial melting. Extending the proposed model to similar late Carboniferous magmatic structures scattered along the southern margin of the Variscan belt requires the existence of a wide, 1500–3000-km-long network of lithosphere-scale shear zones. This structure is able to explain the complex rotation paths reconstructed for the southern Variscides and the crystalline massifs scattered along the Alpine chain, and provides a self-consistent model for HT metamorphism and anatexis during the displacement of paleo-Europe relative to Gondwana.

Acknowledgements

Dr. F. Mantovani (INFN, Italy) is greatly acknowledged for help with measuring U-Th-K abundances, and for a thorough statistical analysis of the geochemical datasets. Comments provided by B. Bonin and J. Alcock greatly improved the presentation of our model. This study was partly supported by grants PRIN Oggiano 2008.

References

Alcock, J.E., Martinez Catalan, J.R., Arenas, R., Diez Montes, A., 2009. Use of thermal modeling to assess the tectono-metamorphic history of the Lugo and Sanabria Domes, Northwest Iberia. Bulletin de la Societe Geologique de France 180, 179-197.

Archanjo, C.J., Hollanda, M.H.B.M., Rodrigues, S.W.O., Neves, B.B.B., Armstrong, R., 2008. Fabrics of pre- and syntectonic granite plutons and chronology of shear zones in the Eastern Borborema Province, NE Brazil. Journal of Structural Geology 30, 310-326.

Archanjo, C.J., Viegas, L.G.F., Hollanda, M.H.B.M., Souza, L.C., Liu, D., 2013. Timing of the HT/LP transpression in the Neoproterozoic Seridó Belt (Borborema Province, Brazil): Constraints from UPb (SHRIMP) geochronology and implications for the connections between NE Brazil and West Africa. Gondwana Research 23, 701-714.

Barbey, P., Gasquet, D., Pin, C., Bourgeix, A.L., 2008. Igneous banding, schlieren and mafic enclaves in calc-alkaline granites: The Budduso pluton (Sardinia). Lithos 104, 147-163.

Bellot, J.-P., 2007. Pre- to syn-extension melt-assisted nucleation and growth of extensional gneiss domes: The western French Massif Central (Variscan belt). Journal of Structural Geology 29, 863-880.

Ben-Zion, Y., Sammis, C.G., 2012. Shear heating during distributed fracturing and pulverization of rocks. Geology 41, 139-142.

Bonin, B., 2004. Do coeval mafic and felsic magmas in post-collisional to within-plate regimes necessarily imply two contrasting, mantle and crustal, sources? A review. Lithos 78, 1-24.

Bonin, B., Azzouni-Sekkal, A., Bussy, F., Ferrag, S., 1998. Alkali-calcic and alkaline post-orogenic (PO) granite magmatism: petrologic constraints and geodynamic settings. Lithos 45, 45-70.

Brouwer, F.M., van de Zedde, D.M.A., Wortel, M.J.R., Vissers, R.L.M., 2004. Late-orogenic heating during exhumation: Alpine PTt trajectories and thermomechanical models. Earth and Planetary Science Letters 220, 185-199.

Burg, J.P., Gerya, T.V., 2005. The role of viscous heating in Barrovian metamorphism of collisional orogens: thermomechanical models and application to the Lepontine Dome in the Central Alps. Journal of Metamorphic Geology 23, 75-95.

Caggianelli, A., Prosser, G., 2003. Modelling the thermal perturbation of the continental crust after intraplating of thick granitoid sheets: a comparison with the crustal sections in Calabria (Italy). Geological Magazine 139, 699-706.

Carmignani, L., Barca, S., Disperati, L., Fantozzi, P.L., Funedda, A., Oggiano, G., Pasci, S., 1994. Tertiary compression and extension in the Sardinian basement. Bollettino di Geofisica Teorica e Applicata 36, 45-62.

Carosi, R., Montomoli, C., Tiepolo, M., Frassi, C., 2012. Geochronological constraints on post-collisional shear zones in the Variscides of Sardinia (Italy). Terra Nova 24, 42-51.

Carosi, R., Oggiano, G., 2002. Transpressional deformation in northwestern Sardinia (Italy): insights on the tectonic evolution of the Variscan Belt. Comptes Rendus Geoscience 334, 287-294.

Casini, L., 2012. A MATLAB-derived software (geothermMOD1.2) for one-dimensional thermal modeling, and its application to the Corsica-Sardinia batholith. Computers & Geosciences 45, 82-86.

Casini, L., Cuccuru, S., Maino, M., Oggiano, G., Puccini, A., Rossi, P., 2014. Structural map of Variscan northern Sardinia (Italy). Journal of Maps, 1-10.

Casini, L., Cuccuru, S., Maino, M., Oggiano, G., Tiepolo, M., 2012. Emplacement of the Arzachena Pluton (Corsica–Sardinia Batholith) and the geodynamics of incoming Pangaea. Tectonophysics 544-545, 31-49.

Casini, L., Funedda, A., 2014. Potential of pressure solution for strain localization in the Baccu Locci Shear Zone (Sardinia, Italy). Journal of Structural Geology 66, 188-204.

Casini, L., Funedda, A., Oggiano, G., 2010. A balanced foreland-hinterland deformation model for the Southern Variscan belt of Sardinia, Italy. Geological Journal 45, 634-649.
Casini, L., Oggiano, G., 2008. Late orogenic collapse and thermal doming in the northern Gondwana margin incorporated in the Variscan Chain: A case study from the Ozieri Metamorphic Complex, northern Sardinia, Italy. Gondwana Research 13, 396-406.

Casini, L., Puccini, A., Cuccuru, S., Maino, M., Oggiano, G., 2013. GEOTHERM: A finite difference code for testing metamorphic P–T–t paths and tectonic models. Computers & Geosciences 59, 171-180.

Cocherie, A., 1984. Interaction manteau–croûte: son rôle dans la genèse d'associations plutoniques calco-alcalines, contraintes géochimiques (éléments en traces et isotopes du strontium et de l'oxygène). Rennes, p. 245.

Cocherie, A., Rossi, P., Fanning, C.M., Guerrot, C., 2005. Comparative use of TIMS and SHRIMP for U–Pb zircon dating of A-type granites and mafic tholeiitic layered complexes and dykes from the Corsican Batholith (France). Lithos 82, 185-219.

Cocherie, A., Rossi, P., Fouillac, A.M., Vidal, P., 1994. Crust and mantle contributions to granite genesis — An example from the Variscan batholith of Corsica, France, studied by trace-element and Nd-Sr-O-isotope systematics. Chemical Geology 115, 173-211.

Conti, P., Carmignani, L., Funedda, A., 2001. Change of nappe transport direction during the Variscan collisional evolution of central-southern Sardinia (Italy). Tectonophysics 332, 255-273.

Cruciani, G., Franceschelli, M., Jung, S., Puxeddu, M., Utzeri, D., 2008. Amphibole-bearing migmatites from the Variscan Belt of NE Sardinia, Italy: Partial melting of mid-Ordovician igneous sources. Lithos 105, 208-224.

de Souza, Z.S., Montel, J.-M., Gioia, S.M.L.C., Maia de Hollanda, M.H.B., Leite do Nascimento, M.A., Jardim de Sá, E.F., Amaro, V.E., Pimentel, M.M., Lardeaux, J.-M., Veschambre, M., 2006. Electron microprobe dating of monazite from high-T shear zones in the São José de Campestre Massif, NE Brazil. Gondwana Research 9, 441-455.

Del Moro, A., Di Simplicio, P., Ghezzo, C., Guasparri, G., Rita, F., Sabatini, G., 1975. Radiometric data and intrusive sequence in the Sardinian Batholith. Neues Jahrbuch für Mineralogie 126, 28-44.
Di Vincenzo, G., 2004. The Relationship between Tectono-metamorphic Evolution and Argon Isotope Records in White Mica: Constraints from in situ ^{40}Ar-^{39}Ar Laser Analysis of the Variscan Basement of Sardinia. Journal of Petrology 45, 1013-1043.

Di Vincenzo, G., Andriessen, P.A.M., Ghezzo, C., 1996. Evidence of Two Different Components in a Hercynian Peraluminous Cordierite-bearing Granite: the San Basilio Intrusion (Central Sardinia, Italy). Journal of Petrology 37, 1175-1206.

Echtler, H., Malavieille, J., 1990. Extensional tectonics, basement uplift and Stephano-Permian collapse basin in a late Variscan metamorphic core complex (Montagne Noire, Southern Massif Central). Tectonophysics 177, 125-138.

Edel, J.B., 1980. Etude paléomagnétique en Sardaigne – Conséquences pour la géodynamique de la Méditerranée occidentale. Strasbourg, p. 310.

Edel, J.B., Casini, L., Oggiano, G., Rossi, P., Schulmann, K., 2014. Early Permian 90 clockwise rotation of the Maures-Esterel-Corsica-Sardinia block confirmed by new palaeomagnetic data and followed by a Triassic 60 clockwise rotation. Geological Society, London, Special Publications 405, 333-361.
Egeberg, A.T., Bonin, B., Sørensen, H., 1993. The Bonifatto peralkaline granites NW Corsica: a possible case of evolution through volatile transfer. Bulletin de la Societe Geologique de France 164, 739-758.

Faure, M., Cocherie, A., Mézème, E.B., Charles, N., Rossi, P., 2010. Middle Carboniferous crustal melting in the Variscan Belt: New insights from U–Th–Pbtot. monazite and U–Pb zircon ages of the Montagne Noire Axial Zone (southern French Massif Central). Gondwana Research 18, 653-673.

Ferrara, G., Ricci, C.A., Rita, F., 1978. Isotopic ages and tectono-metamorphic history of the metamorphic basement of North-Eastern Sardinia. Contributions to Mineralogy and Petrology 68, 99-106.
Ferré, E.C., Leake, B.E., 2001. Geodynamic significance of early orogenic high-K crustal and mantle melts: example of the Corsica Batholith. Lithos 59, 47-67.

Finetti, I.R., 2005. CROP Project, 1st Edition: Deep Seismic Exploration of the Central Mediterranean and Italy, Amsterdam.

Gaggero, L., Oggiano, G., Buzzi, L., Slejko, F.F., Cortesogno, L., 2007. Post-variscan mafic dikes from the late orogenic collapse to the Tethyan rift : Evidence from Sardinia. Ofioliti 32, 15-37.

Gattacceca, J., Orsini, J.B., Bellot, J.P., Henry, B., Rochette, P., Rossi, P., Cherchi, G., 2004. Magnetic fabric of granitoids from Southern Corsica and Northern Sardinia and implications for Late Hercynian tectonic setting. Journal of the Geological Society 161, 277-289.

Giacomini, F., Bomparola, R.M., Ghezzo, C., 2005. Petrology and geochronology of metabasites with eclogite facies relics from NE Sardinia: constraints for the Palaeozoic evolution of Southern Europe. Lithos 82, 221-248.

Giacomini, F., Bomparola, R.M., Ghezzo, C., Guldbransen, H., 2006. The geodynamic evolution of the Southern European Variscides: constraints from the U/Pb geochronology and geochemistry of the lower

Palaeozoic magmatic-sedimentary sequences of Sardinia (Italy). Contributions to Mineralogy and Petrology 152, 19-42.

Giacomini, F., Dallai, L., Carminati, E., Tiepolo, M., Ghezzo, C., 2008. Exhumation of a Variscan orogenic complex: insights into the composite granulitic–amphibolitic metamorphic basement of south-east Corsica (France). Journal of Metamorphic Geology 26, 403-436.

Gleason, G.C., Tullis, J., 1995. A flow law for dislocation creep of quartz aggregates determinedwith the molten salt cell. Tectonophysics 247, 1-23.

Grad, M., Tiira, T., 2009. The Moho depth map of the European Plate. Geophysical Journal International 176, 279-292.

Guimarães, I.P., Silva Filho, A.F., Almeida, C.N., Macambira, M.B., Armstrong, R., 2011. U–Pb SHRIMP data constraints on calc-alkaline granitoids with 1.3–1.6 Ga Nd TDM model ages from the central domain of the Borborema province, NE Brazil. Journal of South American Earth Sciences 31, 383-396.

Handy, M.R., 1994. Flow laws for rocks containing two non-linear viscous phases: A phenomenological approach. Journal of Structural Geology 16, 287-301.

Hollanda, M.H.B.M., Archanjo, C.J., Souza, L.C., Armstrong, R., Vasconcelos, P.M., 2010. Cambrian mafic to felsic magmatism and its connections with transcurrent shear zones of the Borborema Province (NE Brazil): Implications for the late assembly of the West Gondwana. Precambrian Research 178, 1-14.
Huw Davies, J., von Blanckenburg, F., 1995. Slab breakoff: A model of lithosphere detachment and its test in the magmatism and deformation of collisional orogens. Earth and Planetary Science Letters 129, 85-102.

Ishihara, S., 1981. The granitoid series and mineralization. Economic Geology 75th Anniversary Volume, 458-484.

Johannes, W., Holtz, F., 1996. Petrogenesis and experimental petrology of granitic rocks. Minerals and rocks, Berlin.

Johnson, S.E., Fletcher, J.M., Fanning, C.M., Vernon, R.H., Paterson, S.R., Tate, M.C., 2003. Structure, emplacement and lateral expansion of the San José tonalite pluton, Peninsular Ranges batholith, Baja California, México. Journal of Structural Geology 25, 1933-1957.

Johnson, S.E., Schmidt, K.L., Tate, M.C., 2002. Ring complexes in the Peninsular Ranges Batholith, Mexico and the USA: magma plumbing systems in the middle and upper crust. Lithos 61, 187-208.

Kruhl, J.H., Vernon, R.H., 2005. Syndeformational Emplacement of a Tonalitic Sheet-Complex in a Late-Variscan Thrust Regime: Fabrics and Mechanism of Intrusion, Monte'e Senes, Northeastern Sardinia, Italy. The Canadian Mineralogist 43, 387-407.

Laporte, D., Fernandez, A., Orsini, J.B., 1991. Le complexe d'Ile Rousse, Balagne, Corse du Nord-Ouest : pétrologie et cadre de mise en place des granitoides magnésiopotassiques. Géologie de la France 4, 15-30.

Lewis, J.L., Day, S.M., Magistrale, H., Castro, R.R., Astiz, L., Rebollar, C., Eakins, J., Vernon, F.L., Brune, J.N., 2001. Crustal thickness of the Peninsular Ranges and Gulf Extensional Province in the Californias. Journal of Geophysical Research 106, 13599-13611.

Lexa, O., Schulmann, K., Janoušek, V., Štípská, P., Guy, A., Racek, M., 2011. Heat sources and trigger mechanisms of exhumation of HP granulites in Variscan orogenic root. Journal of Metamorphic Geology 29, 79-102.

Li, X., Lin, W., Faure, M., 2012. SIMS U-Pb zircon dating of migmatites and high Mg-K intrusions from the Variscan orogenic complex of Corsica: from crustal anatexis to mantle melting. Géologie de la France 1, 138.

Lipman, P.W., 1992. Magmatism in the Cordilleran United States; Progress and problems, in: Burchfiel, B.C., Lipman, P.W., Zoback, M.L. (Ed.), The Cordilleran Orogen: conterminous U.S. The Geology of North America, Boulder, CO, pp. 481-514.

Liu, M., 2001. Cenozoic extension and magmatism in the North American Cordillera: the role of gravitational collapse. Tectonophysics 342, 407-433.

Lucazeau, F., Mailhe, D., 1986. Heat flow, heat production and fission track data from the Hercynian basement around the Provençal Basin (Western Mediterranean). Tectonophysics 128, 335-356.

Mancktelow, N.S., 2002. Finite-element modelling of shear zone development in viscoelastic materials and its implications for localisation of partial melting. Journal of Structural Geology 24, 1045-1053.

Matte, P., 2001. The Variscan collage and orogeny (480-290 Ma) and the tectonic definition of the Armorica microplate: a review. Terra Nova 13, 122-128.

Nabelek, P.I., Liu, M., 1999. Leucogranites in the Black Hills of South Dakota: The consequence of shear heating during continental collision. Geology 27, 523-526.
O'Brien, P.J., Rotzler, J., 2003. High-pressure granulites: formation, recovery of peak conditions and implications for tectonics. Journal of Metamorphic Geology 21, 3-20.

Oggiano, G., Casini, L., Mameli, P., Rossi, P., 2007. Long lived dextral strike-slip tectonics in the southern Variscan Belt: evidence from two syn-kynematic intrusions in north Sardinia. Géologie de la France 2, 142.

Oggiano, G., Cherchi, G.P., Aversano, A., Di Pisa, A., Ulzega, A., Orrù, P., Pintus, C., 2005. Note Illustrative della Carta Geologica d'Italia alla scala 1:50000, Foglio 428, Arzachena, Firenze.

Orsini, J.B., 1976. Les granitoides hercyniens corse-sardes: mise en évidence des deux associations magmatiques. Bulletin de la Société Géologique de France 18, 1203-1206.

Paquette, J.L., Ménot, R.-P., Pin, C., Orsini, J.B., 2003. Episodic and short-lived granitic pulses in a post-collisional setting: evidence from precise U–Pb zircon dating through a crustal cross-section in Corsica. Chemical Geology 198, 1-20.

Paterson, S.R., Vernon, R.H., Tobisch, O.T., 1989. A review of criteria for the identification of magmatic and tectonic foliations in granitoids. Journal of Structural Geology 11, 349-363.

Patino Douce, A.E., 2004. Vapor-Absent Melting of Tonalite at 15-32 kbar. Journal of Petrology 46, 275-290.

Pereira, M.F., Apraiz, A., Chichorro, M., Silva, J.B., Armstrong, R.A., 2010. Exhumation of high-pressure rocks in northern Gondwana during the Early Carboniferours (Coimbra–Cordoba shear zone, SW Iberian Massif): Tectonothermal analysis and U–Th–Pb SHRIMP in-situ zircon geochronology. Gondwana Research 17, 440-460.

Petford, N., Cruden, A.R., McCaffrey, K.J.W., Vigneresse, J.L., 2000. Nature 408, 669-673.

Platt, J.P., Behr, W.M., 2011. Lithospheric shear zones as constant stress experiments. Geology 39, 127-130.

Poitrasson, F., Duthou, J.L., Pin, C., 1995. The Relationship between Petrology and Nd Isotopes as Evidence for Contrasting Anorogenic Granite Genesis: Example of the Corsican Province (SE France). Journal of Petrology 36, 1251-1274.

Poitrasson, F., Paquette, J.-L., Montel, J.-M., Pin, C., Duthou, J.-L., 1998. Importance of late-magmatic and hydrothermal fluids on the Sm–Nd isotope mineral systematics of hypersolvus granites. Chemical Geology 146, 187-203.

Poli, G., Ghezzo, C., Conticelli, S., 1989. Geochemistry of granitic rocks from the Hercynian Sardinia-Corsica batholith: Implication for magma genesis. Lithos 23, 247-266.

Poli, G., Tommasini, S., 1991. A geochemical approach to the evolution of granitic plutons: a case study, the acid intrusions of Punta Falcone (northern Sardinia, Italy). Chemical Geology 92, 87-105.

Poli, G., Tommasini, S., 1999. Geochemical modeling of acid–basic magma interaction in the Sardinia–Corsica Batholith: the case study of Sarrabus, southeastern Sardinia, Italy. Lithos 46, 553-571.

Ranalli, G., 1995. Rheology of the Earth. Springer Science & Business Media.

Ray, L., Forster, H., Schilling, F., Forster, A., 2006. Thermal diffusivity of felsic to mafic granulites at elevated temperatures. Earth and Planetary Science Letters 251, 241-253.
Renna, M.R., Tribuzio, R., Braga, R., 2013. Petrogenetic relationships between peralkaline rhyolite dykes and mafic rocks in the post-Variscan gabbroic complex from Bocca di Tenda (northern Corsica, France). Contributions to Mineralogy and Petrology 165, 1073-1085.

Renna, M.R., Tribuzio, R., Tiepolo, M., 2006. Interaction between basic and acid magmas during the latest stages of the post-collisional Variscan evolution: Clues from the gabbro–granite association of Ota (Corsica–Sardinia batholith). Lithos 90, 92-110.

Renna, M.R., Tribuzio, R., Tiepolo, M., 2007. Origin and timing of the post-Variscan gabbro–granite complex of Porto (Western Corsica). Contributions to Mineralogy and Petrology 154, 493-517.

Rossi, P., Chavez, J.Y., Cocherie, A., 1988. Age varisque précoce du plutonisme magnésio-potassique en Corse occidentale : conséquences géodynamiques. Comptes rendus de l'Académie des sciences 307, 1541-1547.

Rossi, P., Cocherie, A., 1991. Genesis of a Variscan batholith: Field, petrological and mineralogical evidence from the Corsica-Sardinia batholith. Tectonophysics 195, 319-346.

Rossi, P., Oggiano, G., Cocherie, A., 2009. A restored section of the “southern Variscan realm” across the Corsica–Sardinia microcontinent. Comptes Rendus Geoscience 341, 224-238.

Rubatto, D., Ferrando, S., Compagnoni, R., Lombardo, B., 2010. Carboniferous high-pressure metamorphism of Ordovician protoliths in the Argentera Massif (Italy), Southern European Variscan belt. Lithos 116, 65-76.

Sá, J.M., Bertrand, J.M., Leterrier, J., Macedo, M.H.F., 2002. Geochemistry and geochronology of pre-Brasiliano rocks from the Transversal Zone, Borborema Province, Northeast Brazil. Journal of South American Earth Sciences 14, 851-866.

Secchi, F.A., Brotzu, P., Callegari, E., 1991. The Arburese igneous complex (SW Sardinia, Italy) — an example of dominant igneous fractionation leading to peraluminous cordierite-bearing leucogranites as residual melts. Chemical Geology 92, 213-249.

Silver, L.T., Chappell, B.W., 1988. The Peninsular Ranges Batholith: an insight into the evolution of the Cordilleran batholiths of southwestern North America. Transactions of the Royal Society of Edinburgh: Earth Sciences 79, 105-121.

Tommasini, S., Poli, G., 1992. Petrology of the late-Carboniferous Punta Falcone gabbroic complex, nothern Sardinia, Italy. Contributions to Mineralogy and Petrology 110, 16-32.

Tribuzio, R., Renna, M.R., Braga, R., Dallai, L., 2009. Petrogenesis of Early Permian olivine-bearing cumulates and associated basalt dykes from Bocca di Tenda (Northern Corsica): Implications for post-collisional Variscan evolution. Chemical Geology 259, 190-203.

Turcotte, D.L., Schubert, G., 2002. Geodynamics. Cambridge University Press, Cambridge, UK.

Verdoya, M., Pasquale, V., Chiozzi, P., Kukkonen, I.T., 1998. Radiogenic heat production in the Variscan crust: new determinations and distribution models in Corsica (northwestern Mediterranean). Tectonophysics 291, 63-75.

Vilà, M., Pin, C., Enrique, P., Liesa, M., 2005. Telescoping of three distinct magmatic suites in an orogenic setting: Generation of Hercynian igneous rocks of the Albera Massif (Eastern Pyrenees). Lithos 83, 97-127.
Vogt, K., Gerya, T.V., Castro, A., 2012. Crustal growth at active continental margins: Numerical modeling. Physics of the Earth and Planetary Interiors 192-193, 1-20.

von Raumer, J.F., Bussy, F., Schaltegger, U., Schulz, B., Stampfli, G.M., 2012. Pre-Mesozoic Alpine basements--Their place in the European Paleozoic framework. Geological Society of America Bulletin 125, 89-108.

Vosteen, H.-D., Schellschmidt, R., 2003. Influence of temperature on thermal conductivity, thermal capacity and thermal diffusivity for different types of rock. Physics and Chemistry of the Earth, Parts A/B/C 28, 499-509.

Whittington, A.G., Hofmeister, A.M., Nabelek, P.I., 2009. Temperature-dependent thermal diffusivity of the Earth's crust and implications for magmatism. Nature 458, 319-321.

Figure captions

Fig. 1. Geological setting of the C-SB: (**a**) structural sketch map of Variscan Europe, CIZ, Central Iberian Zone, MC, French Massif Central, MGCR, Mid-German Crystalline Rise, ECM, External Crystalline Massif, BM, Bohemian Massif, C-S, Corsica-Sardinia (modified from Matte (2001)), (**b**) Bouguer anomaly map of the Corsica-Sardinia block (redrawn from Grad and Tiira (2009)), the dashed area represents the C-SB, (**c**) structural-petrographic sketch map of the C-SB.

Fig. 2. Structure of U2/U3 plutons: (**a**) melt-bearing shear zone in the root zone of U2 plutons (Barrabisa outcrop), (**b**) collection zone of U2 melts (northern Asinara Island), c) foliation-perpendicular sill filled by U2 granodioritic melts (Barrabisa outcrop), d) Fragments of the U2 Arzachena pluton (Casini et al., 2012) enclosed within younger U3 rocks; ages are indicated.

Fig. 3. Volume ratio/age diagram showing the growth rate of the C-SB; blue dots represent dated plutons, AZN, Arzachena pluton (Casini et al., 2012), bb, Barrabisa granodiorite, MgK granites stands for U1 rocks of northern Corsica.

Fig. 4. Summary of geochemical data for U2/U3 rocks, including the MALI (Modified Alkali-Lime Index) diagram, A/CNK diagram and Harker variation diagrams.

Fig. 5. Average REE patterns for U2 (red dots) and U3 (blue dots) rocks; the grey fields represent standard deviation to average composition.

Fig. 6. Compilation of $\varepsilon Nd/SiO_2$ data for U2/U3 rocks.

Fig. 7. Results of numerical experiments: (**a-c**) experiments r1-r5 for constant exhumation rate and shear heating, variable age of slab break off; (**d-f**) experiments r6-10 for constant exhumation rate and age of slab break off, variable shear heating; (**g**) experiment r11 for constantly increasing exhumation rates, slab break off at 345 Ma, 10^{-13} s^{-1} shear strain rate, (**h**) experiment r13 for step-like decreasing exhumation rates, slab break off at 345 Ma, 10^{-13} s^{-1} shear strain rate, (i) results of experiment r18 (best fit to P-T-t data) for constantly decreasing exhumation rates, slab break off at 346 Ma, $10^{-12.9}$ s^{-1} shear strain rate.

Fig. 8. Best fit/age diagram showing the relative error between the calculated geotherm and P-T-t constraints in the range of ages between 350 and 280 Ma.

Fig. 9. Conceptual model for U2 magmatism: (a) plan view of brittle and ductile flow trajectories (solid and dotted lines, respectively). Red ellipses indicate the expected orientation of dilatant sites developed around the brittle-ductile transition zone. SVSZ stand for South Variscan Shear Zone. The inferred geometry and position of both Arzachena and Barrabisa plutons is indicated to illustrate the evolution of U2 magmatic system; (b) 3D geometry of a melt-bearing shear zone, red arrows indicate melt pathways; (c) shear stress profile calculated for the model crust used in thermal models.

Fig. **10.** Geodynamic evolution of the Corsica-Sardinia block in Variscan times – sections are not to scale. The shaded area represents sub-continental mantle lithosphere. Plutons related to the main magmatic suites are shown (U1 – violet, U2 – red, and U3 – pink).

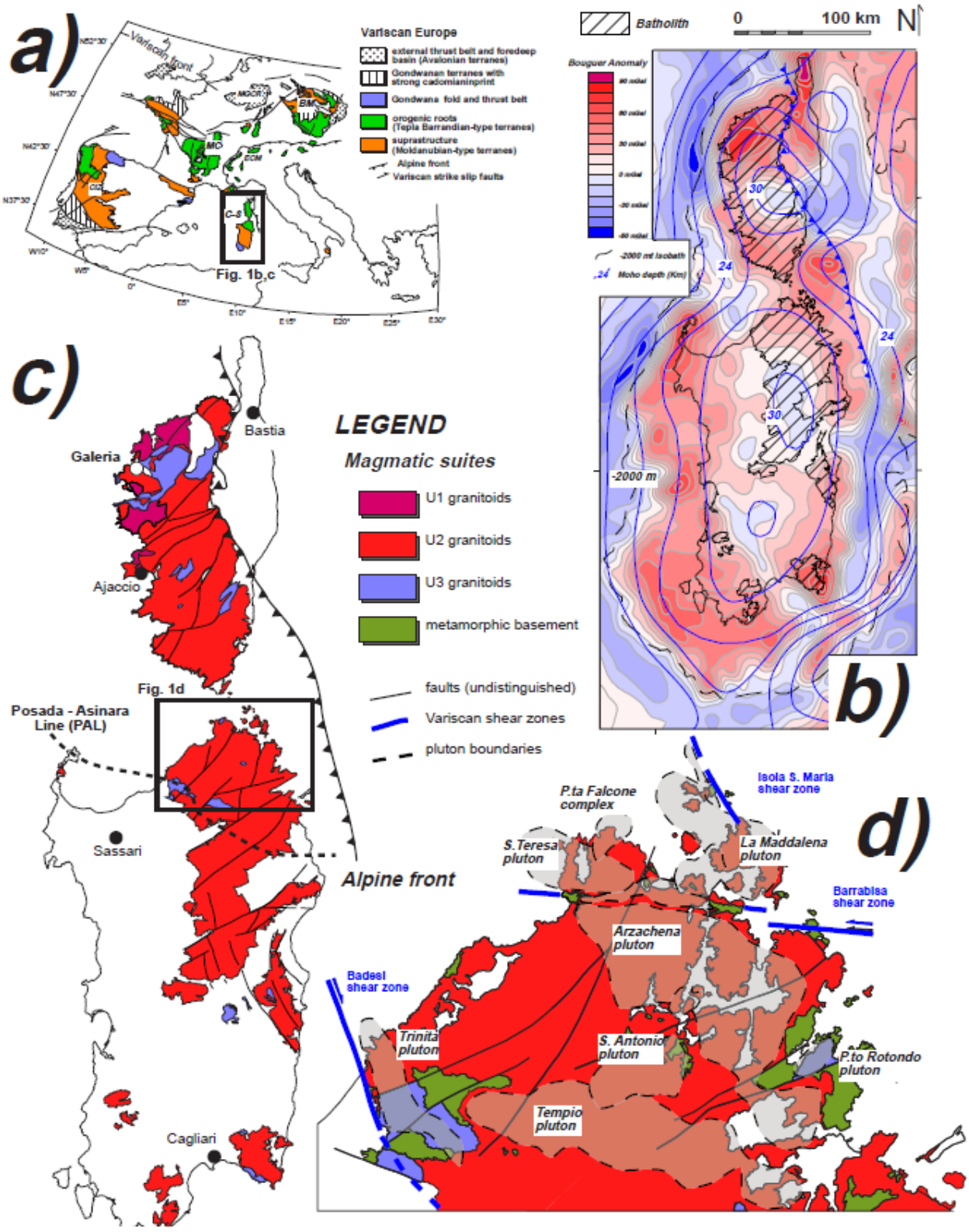
a)
Variscan Europe
external thrust belt and foredeep basin (Avalonian terranes)
Gondwanan terranes with strong cadomianinprint
Gondwana fold and thrust belt
orogenic roots (Tepla Barrandian-type terranes)
suprastructure (Moldanubian-type terranes)
Alpine front
Variscan strike slip faults
Variscan front
MCM
BM
MC
ECM
CB
C-S
Fig. 1b,c
Batholith
0
100 km
N
Bouguer Anomaly
-2000 m isobath
Moho depth (Km)
30
24
-2000 m
b)
c)
LEGEND
Magmatic suites
U1 granitoids
U2 granitoids
U3 granitoids
metamorphic basement
faults (undistinguished)
Variscan shear zones
pluton boundaries
Bastia
Galeria
Ajaccio
Fig. 1d
Posada - Asinara Line (PAL)
Sassari
Alpine front
Cagliari
d)
P.ta Falcone complex
Isola S. Maria shear zone
S.Teresa pluton
La Maddalena pluton
Barrabisa shear zone
Arzachena pluton
Badesi shear zone
Trinita pluton
S. Antonio pluton
P.to Rotondo pluton
Tempio pluton

Fig1

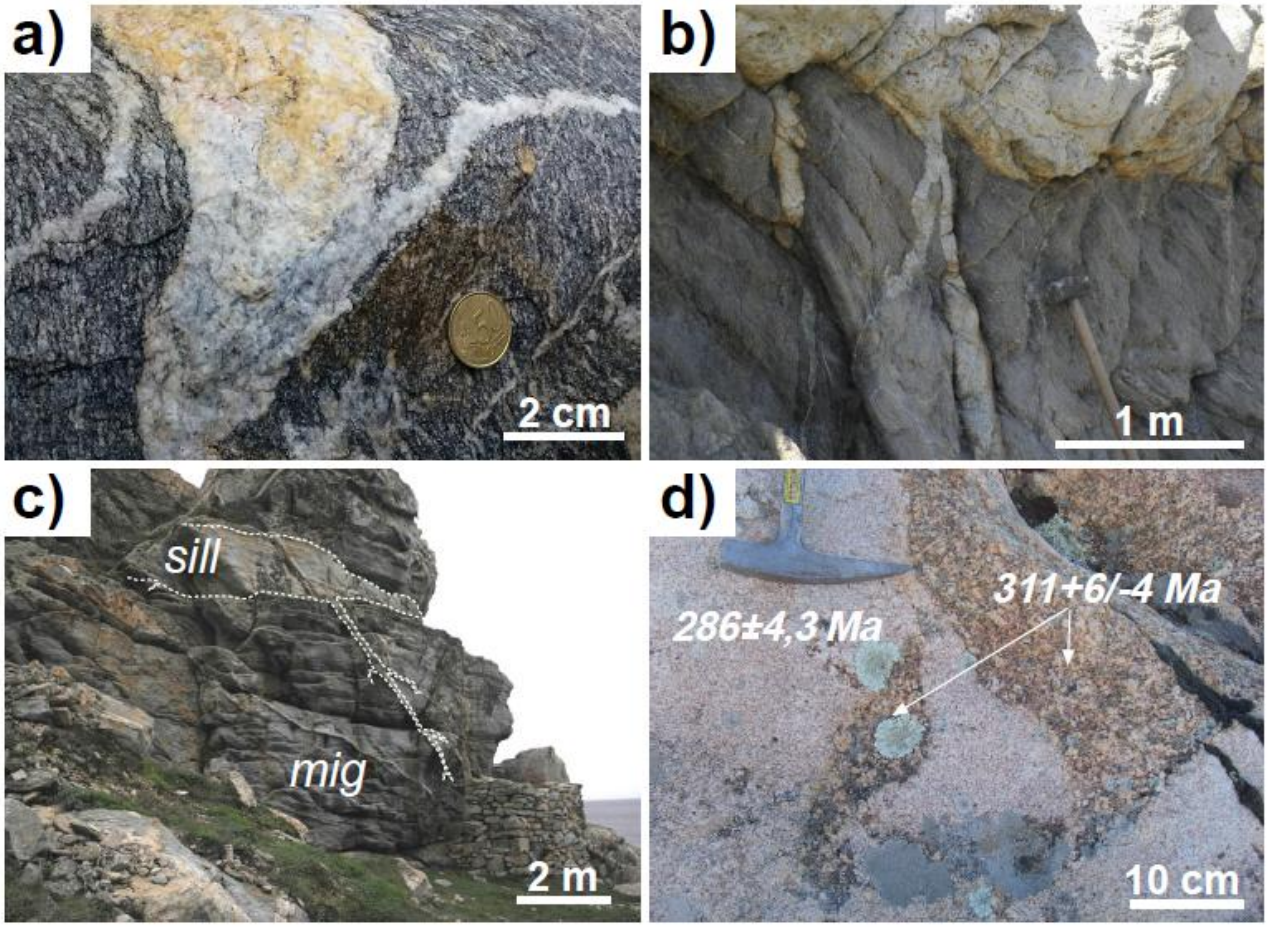
a)
2 cm
b)
1 m
c)
sill
mig
2 m
d)
311+6/-4 Ma
286±4,3 Ma
10 cm

Fig2

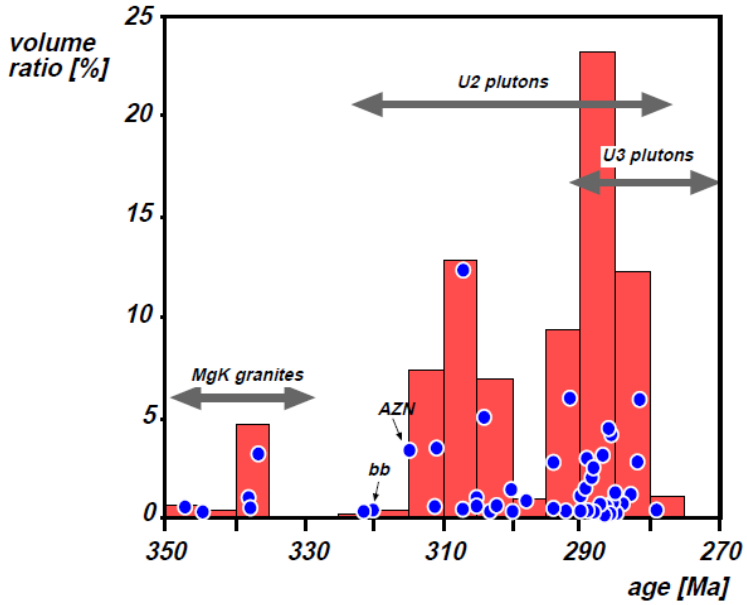
volume ratio [%]
25
20
15
10
5
0
U2 plutons
U3 plutons
MgK granites
AZN
bb
350
330
310
290
270
age [Ma]

Fig3

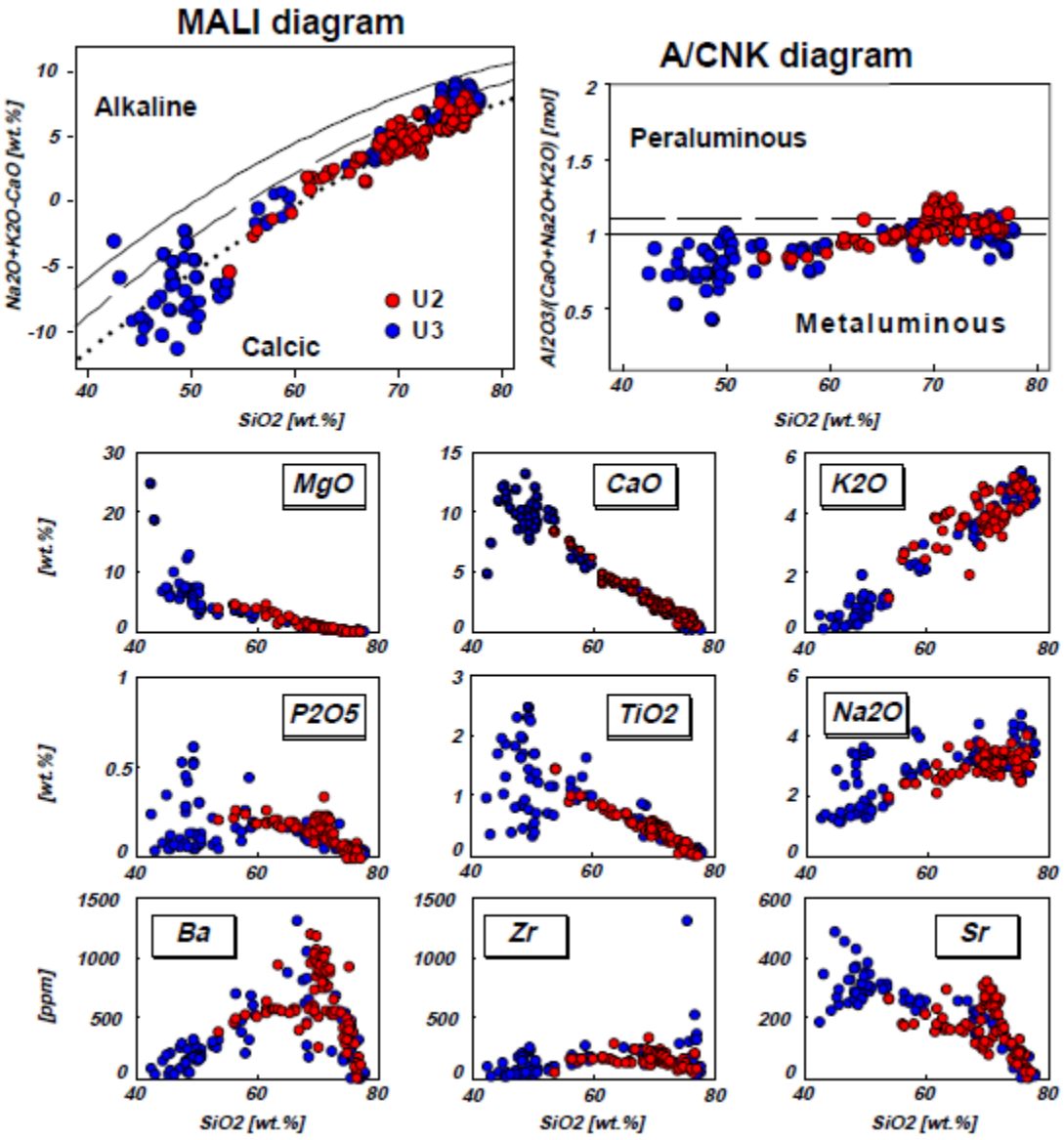
MALI diagram
Alkaline
Calcic
U2
U3
Na2O+K2O-CaO [wt.%]
SiO2 [wt.%]
A/CNK diagram
Peraluminous
Metaluminous
Al2O3/(CaO+Na2O+K2O) [mol]
SiO2 [wt.%]
MgO
CaO
K2O
P2O5
TiO2
Na2O
Ba
Zr
Sr
[wt.%]
[ppm]
SiO2 [wt.%]

Fig4

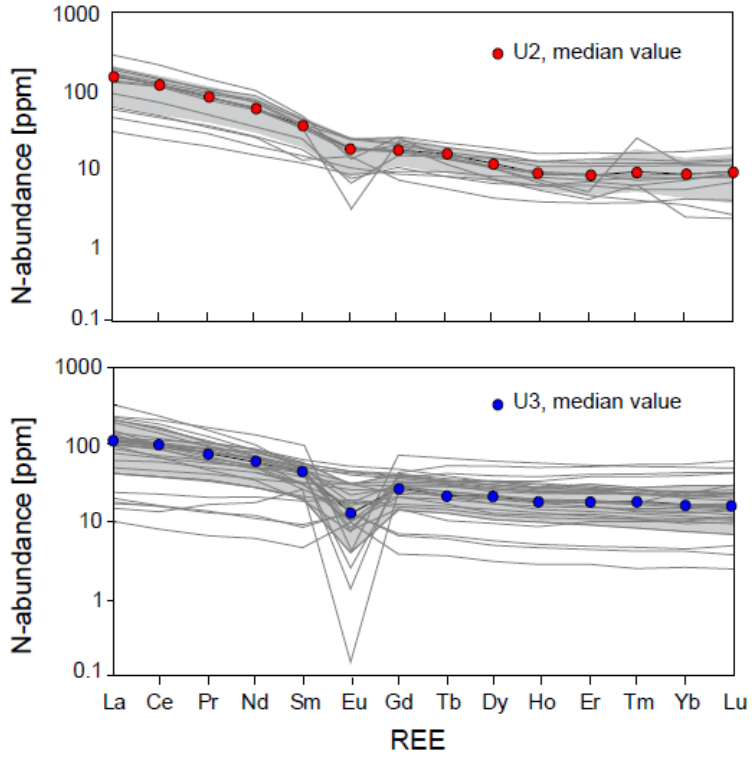
U2, median value
U3, median value
N-abundance [ppm]
1000
100
10
1
0.1
La Ce Pr Nd Sm Eu Gd Tb Dy Ho Er Tm Yb Lu
REE

fig5

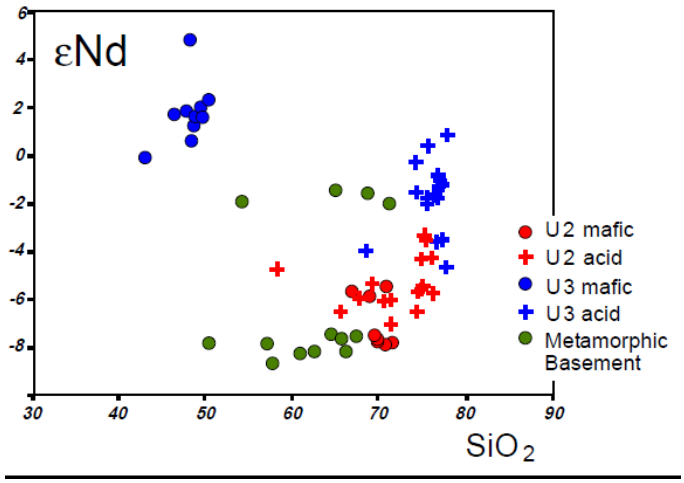
εNd
U2 mafic
U2 acid
U3 mafic
U3 acid
Metamorphic Basement
SiO2

Fig6

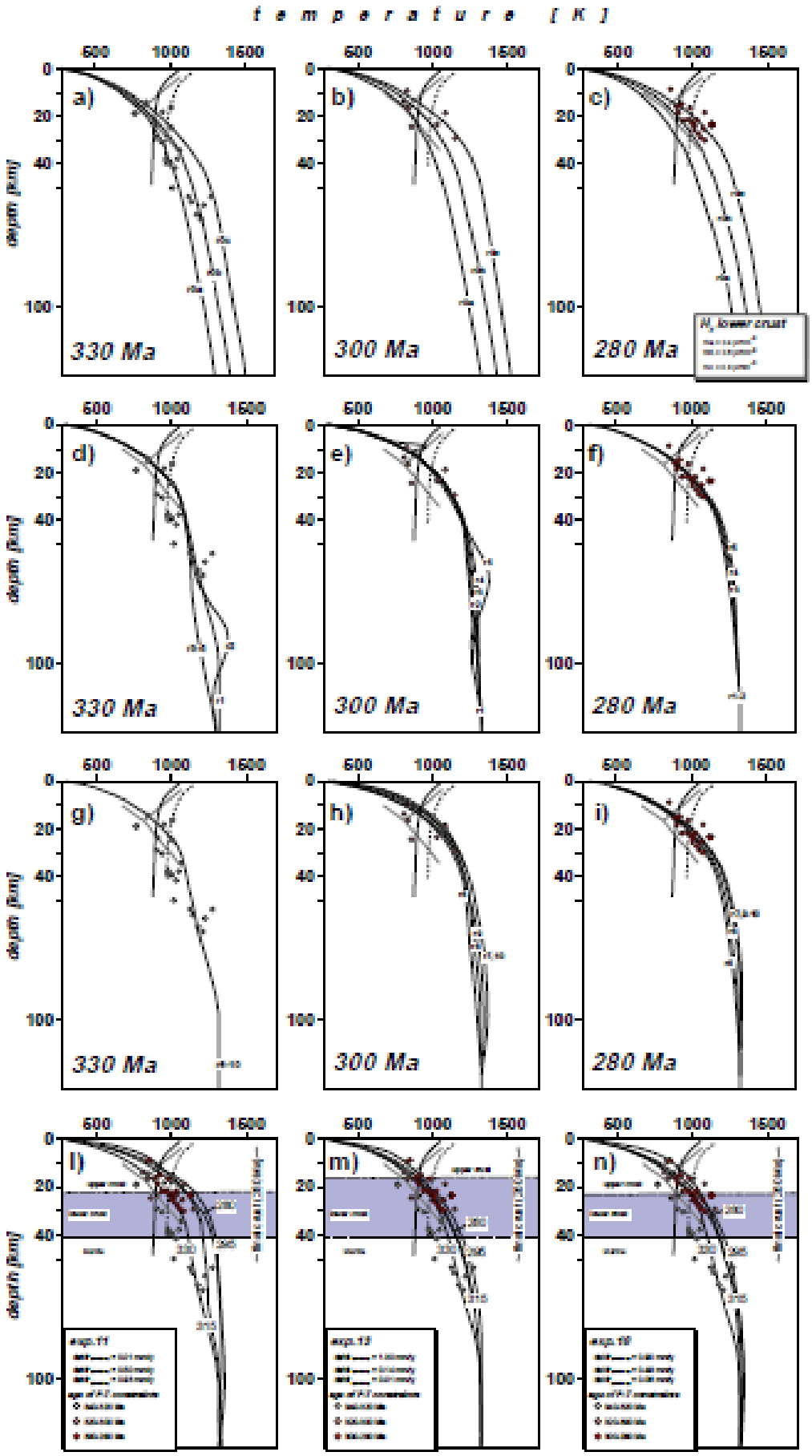
temperature [K]
600
1000
1600
0
20
40
100
depth [km]
a)
330 Ma
b)
300 Ma
c)
280 Ma
d)
330 Ma
e)
300 Ma
f)
280 Ma
g)
330 Ma
h)
300 Ma
i)
280 Ma
l)
m)
n)

Fig7

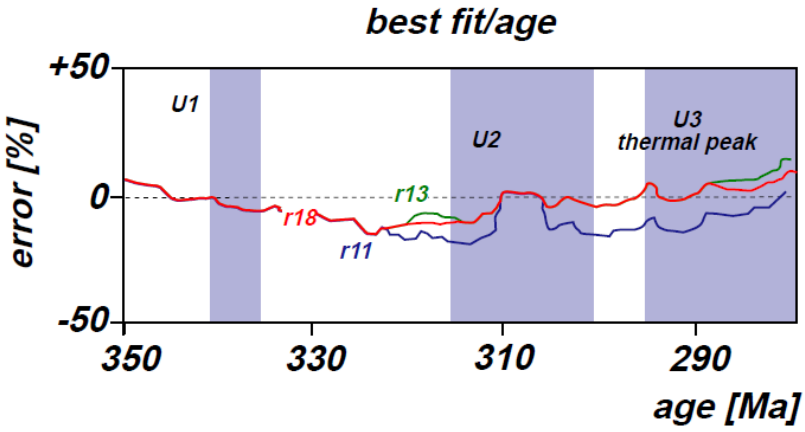
best fit/age
+50
0
-50
error [%]
U1
U2
U3
thermal peak
r13
r18
r11
350
330
310
290
age [Ma]

Fig8

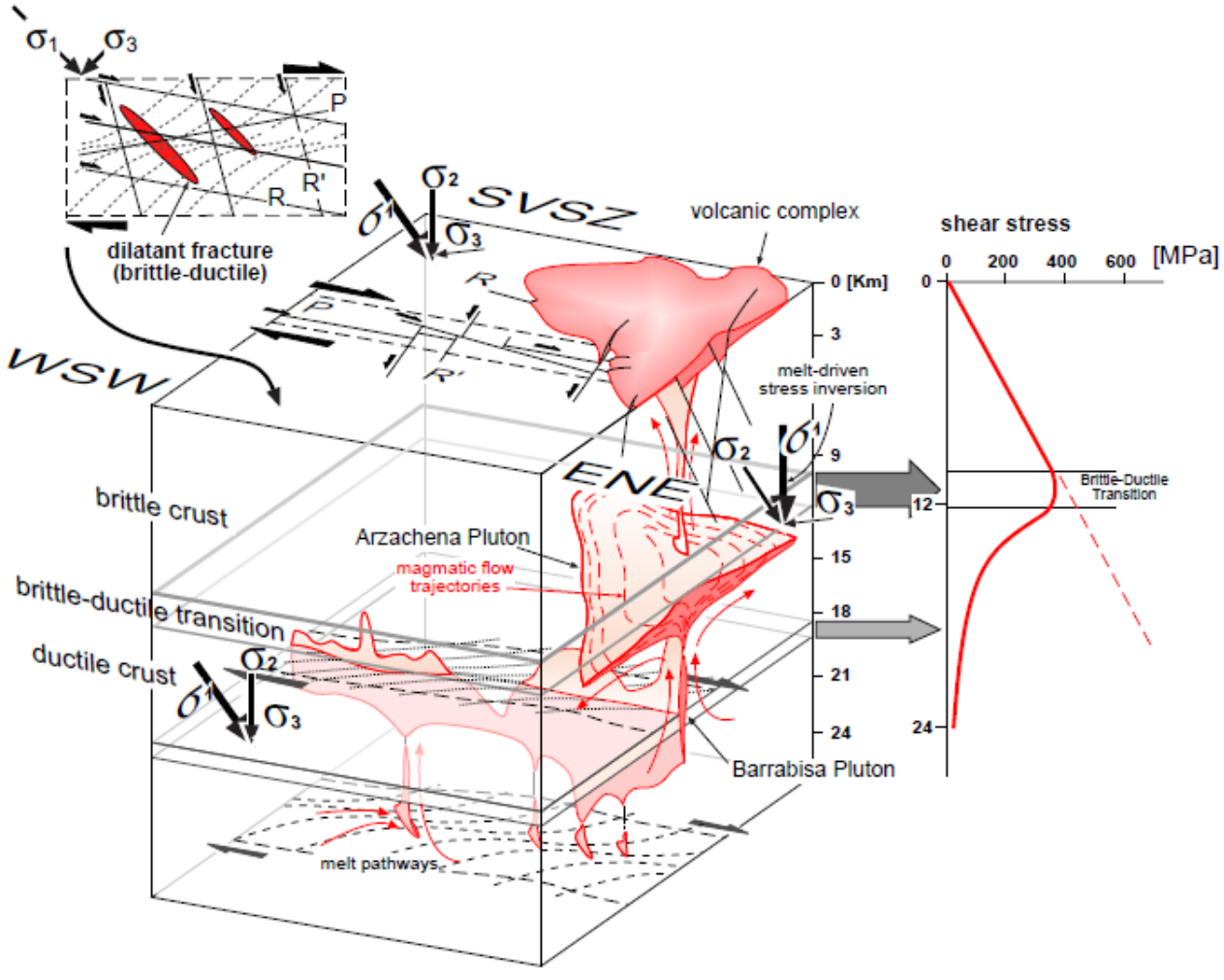
σ1
σ3
P
R
R'
dilatant fracture
(brittle-ductile)
σ2
σ1
σ3
SVSZ
volcanic complex
shear stress
0
200
400
600
[MPa]
0 [Km]
3
9
12
15
18
21
24
melt-driven
stress inversion
Brittle-Ductile
Transition
WSW
ENE
brittle crust
brittle-ductile transition
ductile crust
Arzachena Pluton
magmatic flow
trajectories
Barrabisa Pluton
melt pathways

Fig9

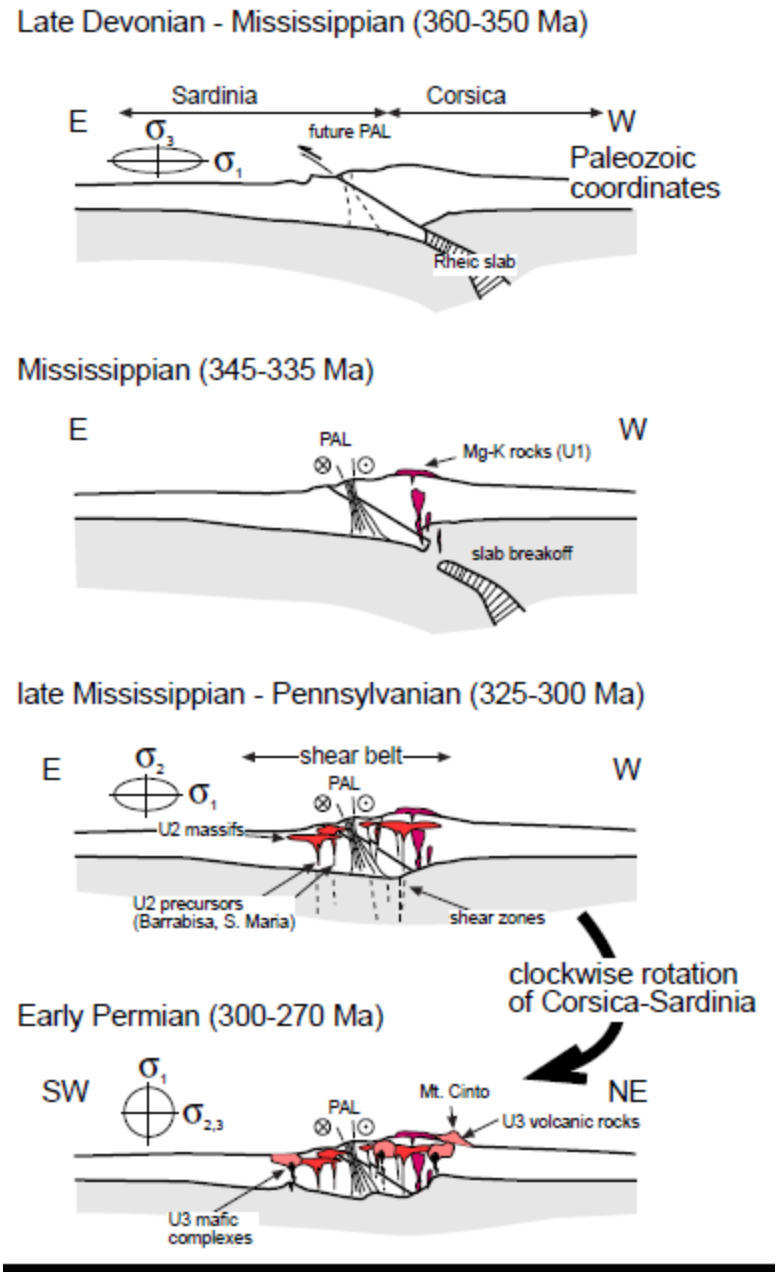
Late Devonian - Mississippian (360-350 Ma)
Sardinia
Corsica
E
W
σ3
σ1
future PAL
Paleozoic
coordinates
Rheic slab
Mississippian (345-335 Ma)
E
W
PAL
Mg-K rocks (U1)
slab breakoff
late Mississippian - Pennsylvanian (325-300 Ma)
E
σ2
σ1
shear belt
W
PAL
U2 massifs
U2 precursors
(Barrabisa, S. Maria)
shear zones
clockwise rotation
of Corsica-Sardinia
Early Permian (300-270 Ma)
SW
σ1
σ2,3
PAL
Mt. Cinto
NE
U3 volcanic rocks
U3 mafic
complexes

Fig10